NASA TM X-174

TECHNICAL MEMORANDUM

X-174

INVESTIGATION OF THE EFFECT OF NACELLES ON THE AERODYNAMIC CHARACTERISTICS OF A CAMBERED AND TWISTED 80° SWEPT ARROW WING AT MACH NUMBERS OF 2.29 AND 2.98

By Dennis F. Hasson and Robert M. Lust

Langley Research Center
Langley Field, Va.

NATIONAL AERONAUTICS AND SPACE ADMINISTRATION
WASHINGTON
January 1960

NATIONAL AERONAUTICS AND SPACE ADMINISTRATION

TECHNICAL MEMORANDUM X-174

INVESTIGATION OF THE EFFECT OF NACELLES ON THE AERODYNAMIC CHARACTERISTICS OF A CAMBERED AND TWISTED 80° SWEPT ARROW WING AT MACH NUMBERS OF 2.29 AND 2.98*

By Dennis F. Hasson and Robert M. Lust

SUMMARY

An investigation has been made to determine the effect of an installation of four nacelles - two underwing and two overwing - on the aerodynamic characteristics of a cambered and twisted wing with a leading-edge sweep of 80°. The aspect ratio of the wing was 1.085, taper ratio of 0, and a notch ratio of 0.65. A 2.5-percent biconvex thickness distribution was utilized about the cambered and twisted wing chord plane.

The investigation was made with transition fixed on the wing surfaces. The Reynolds numbers based on the mean aerodynamic chord were 4.5×10^6.

INTRODUCTION

In recent years there has been much effort devoted to the development of airplane configurations having long-range capabilities at supersonic speeds. Among the configurations investigated were those which are essentially all wing. Camber and twist were incorporated in these wings to obtain the optimum load distribution which linear theory indicates will result in substantial gains in lift-drag ratio. Results of these investigations are reported in references 1 to 3. Since it is probable that some arrangement of nacelles will be required to house the engines of an actual aircraft, two possible combinations of underwing nacelles were included on the model configuration tested in reference 2. This configuration was sized to represent a large, long-range bomber. On a model representing a smaller airplane, it might not be possible to locate all engines below the

*Title, Unclassified.

wing due to the increased size of the engine nacelles relative to the wing. For such an airplane, an overwing location of some of the nacelles is a possibility.

The present investigation is intended to provide an indication of the effect of large nacelles (located above and below the wing) on the aerodynamic characteristics of a cambered and twisted wing having lift-drag ratios of the level required of long-range supersonic aircraft.

SYMBOLS

The longitudinal characteristics of the model are referred to the stability system of axes. The lateral characteristics of the model are referred to the body system of axes. The systems of axes used and the positive direction of forces, moments, and angles are shown in figure 1.

The moments of the model are presented about the 0.617-chord point of the mean aerodynamic chord and on the model reference line.

Symbols used in this paper are defined as follows:

b	wing span, 17.63 in.
$\bar{c}$	wing mean aerodynamic chord, 21.67 in.
C'_D	external drag coefficient, $\frac{\text{Total drag}}{qS} - C'_{D,b} - C'_{D,i}$
$C'_{D,b}$	base drag coefficient, $\frac{\text{Base drag}}{qS}$
$C'_{D,i}$	internal drag coefficient, $\frac{\text{Internal drag}}{qS}$
C_L	lift coefficient, $\frac{\text{Lift}}{qS}$
C_m	pitching-moment coefficient, $\frac{\text{Pitching moment}}{qS\bar{c}}$
C_l	rolling-moment coefficient, $\frac{\text{Rolling moment}}{qSb}$
C_n	yawing-moment coefficient, $\frac{\text{Yawing moment}}{qSb}$
C_Y	side-force coefficient, $\frac{\text{Side force}}{qS}$

C_{L_α}	lift-curve slope ($\alpha \approx 0^\circ$), $\frac{\partial C_L}{\partial \alpha}$ per deg
C_{l_β}	effective dihedral parameter ($\beta \approx 0^\circ$), $\frac{\partial C_l}{\partial \beta}$ per deg
C_{n_β}	directional stability parameter ($\beta \approx 0^\circ$), $\frac{\partial C_n}{\partial \beta}$ per deg
C_{Y_β}	side-force parameter ($\beta \approx 0^\circ$), $\frac{\partial C_Y}{\partial \beta}$ per deg
$\frac{\partial C_m}{\partial C_L}$	pitching-moment curve slope ($C_L \approx 0^\circ$)
$\frac{\partial C_D'}{\partial C_L^2}$	drag-due-to-lift factor, $\frac{C_D' - C_{D,min}'}{C_L^2 \text{ for } (L/D)_{max}}$
L/D	lift-drag ratio, C_L/C_D
M	free-stream Mach number
R	Reynolds number
S	theoretical wing area, 1.99 sq ft
q	free-stream dynamic pressure, lb/sq ft
α	angle of attack referred to a reference line, deg
β	angle of sideslip referred to model plane of symmetry, deg

Subscripts:

max	maximum
min	minimum

MODEL AND APPARATUS

The tests were conducted in the high Mach number test section of the Langley Unitary Plan wind tunnel. The tunnel is a variable-pressure continuous-flow type. The test section is 4 feet square and approximately

7 feet in length. The nozzle leading to the test section is of the asymmetric sliding-block type. Mach numbers may be varied continuously through a Mach range from approximately 2.29 to 4.65 without tunnel shutdown.

A drawing of the model is presented in figure 2 and details of the nacelles are presented in figure 3. Geometric characteristics of the model are given in table I. Ordinates for the surfaces of the cambered and twisted wing are contained in reference 3. Photographs showing the wing with and without nacelles are presented in figures 4 and 5, respectively.

The wing consisted of a 25-percent-thick biconvex airfoil section distributed about the cambered and twisted chordplane. A balance fairing was placed on the upper surface of the wing to house the force and moment sensing balance. The cross section of the balance fairing represents the minimum area obtainable to adequately house the balance. In order to establish a relationship between the size of the wing and the nacelles, a proposed airplane design, similar in configuration to the test model, was used to establish a prototype size and a corresponding scale of the test model. The model nacelles were scaled, both in size and location from the selected prototype nacelle installation enclosing engines of the proposed airplane design. The model nacelles are illustrated in figure 3.

The nacelle installation consisted of four nacelles. One pair of nacelles was located below the wing, one on each side of the balance fairing, and one pair above the wing at the same spanwise location as the underwing installations. The pylons supporting the nacelles were skewed relative to the plane of symmetry in an attempt to obtain alinement with flow over the wing surface.

Forces and moments for the complete model were measured by means of a six-component electrical strain-gage balance. The balance was attached by means of a sting to the tunnel central support system. The moments were measured at a point located at the 61.7 percent of the wing mean aerodynamic chord and on the model reference line.

An additional component of the model support system was a remotely operated adjustable coupling which permitted tests to be performed at variable sideslip angles concurrently with variable angles of attack. This coupling was placed between the model sting and the tunnel central support system.

TESTS

The tests were conducted at the conditions indicated in the following table:

Mach number	2.29	2.98
Reynolds number (based on $\bar{c}$)	4.5×10^6	4.5×10^6
Stagnation pressure, lb/sq in. abs	13.2	19.0
Dynamic pressure, lb/sq ft	566	478
Stagnation temperature, °F	150	150

The dewpoint for all tests was maintained at less than -30° F. The angle-of-attack range was -7° to 11°.

Transition was fixed for all tests. The transition strips consisted of bands of sand 1/32 inch wide applied at 10 percent of the local streamwise chord on the wing upper and lower surface with a density of about 100 grains per square inch. The grain height was 0.011 inch to 0.013 inch.

To indicate flow conditions on the upper surface of the wing, a fluorescent oil was applied to the surface. The flow conditions in the boundary layer produce distinguishing areas of fluorescent oil density on the wing surface. The wing surface, illuminated by ultraviolet light, was photographed and the composite figure of these results is presented in figure 6. A more complete description of this technique is given in reference 4.

CORRECTIONS AND ACCURACY

A calibration of the flow angularity in the test section has shown that there is a small upflow. The degree of flow misalinement was determined by upright and inverted runs of the model at both Mach numbers. The results presented herein have been corrected for this flow misalinement. The maximum deviation of local Mach number for the portion of the test section occupied by the model was ±0.015 from the average values listed.

Pressure measurements were made in the balance cavity and on the base of an upper and lower nacelle over the test angle-of-attack and Mach number ranges. The base pressures and the cavity pressure have been used to

adjust the level of the drag coefficients presented herein to a condition representing free-stream static pressure at the model and nacelle base areas.

The internal duct losses for flow through the nacelles were determined by measurement of static and total pressures near the nacelle exit. Once determined, these losses were used to compute the internal drag coefficients. The internal drag coefficients have been removed from the model drag coefficients presented herein. The base drag coefficients and the internal drag coefficients are presented in figure 7.

The base-pressure adjustment for the plugged nacelle configuration represents separate measurements applied to the entire base of the nacelle including what normally would be the exit. Because of the asymmetric location of the plugged nacelle with respect to the balance center, this Sase-pressure adjustment was also used to correct the moments affected by virtue of plugging the nacelle.

The estimated accuracy of the force and moment coefficients and angles based on calibration and repeatability of data is

C_L	±0.002
C_D'	±0.0005
C_m	±0.0005
C_l	f0.0001
C_n	±0.0001
C_y	±0.0001
α, deg	f0.l
β, deg	f0.l

PRESENTATION OF RESULTS

The results of this investigation are presented in the following figures:

	Figure
Base and internal drag coefficients	7
Schlieren photographs	8
Longitudinal stability characteristics	9
Summary of longitudinal stability characteristics	10
Lateral stability characteristics	11
Lateral stability parameters	12

DISCUSSION

Longitudinal Stability Characteristics

The longitudinal stability characteristics of the model with and without nacelles are summarized in figure 10. The results show that the data obtained on the wing without nacelles in this investigation agree well with the results previously obtained (ref. 3) despite the slightly different Reynolds numbers ($R = 4.5 \times 10^6$ for the present investigation and $R = 5.0 \times 10^6$ in ref. 3). The only disagreement is in the maximum lift-drag ratio at a Mach number of 2.3 which is at present unexplainable and is considered insignificant.

The addition of four nacelles to the wing reduces the maximum lift-drag ratio by about 3.3 at a Mach number of 2.98. This loss is primarily due to the increase in minimum drag produced by the nacelles ($\Delta C_{D,min}$ due to nacelles of about 0.0170 at a Mach number of 2.98). Undoubtedly, this large increase in minimum drag could be decreased by decreasing the lip angle of the external compression inlet or going to an internal compression inlet design.

The drag due to lift is unchanged at $M = 2.29$ and reduced at $M = 2.98$ by the addition of the nacelles. This is probably due to the large interference of the nacelles on the wing. Hence, the nacelles, in introducing a high level of wave drag, probably minimize the increase in adverse boundary-layer growth associated with increasing lift on the wing alone. The extent of the nacelle wave drag is illustrated by the schlieren photographs (fig. 8). Despite the erroneous lift coefficient ($C_L \approx -0.1$) at which the oil-flow photograph was taken, it is believed to be illustrative of the flow caused by the nacelle, although the degree of inlet compression wave interference is incorrect as shown in the picture. The interference of the nacelle inlet compression waves with the wing surface is represented by the dark areas immediately below the nacelles on the oil-film photograph (fig. 6.).

The plugged nacelle configuration (upper left), which represents a no-flow condition, further increases the minimum drag coefficient (0.0040 at $M = 2.98$) due to the increased wave drag of the solid nacelle. It should be noted here that drag coefficients presented for the plugged nacelle, although having no internal flow loss, have been adjusted to a level of free-stream static pressure over the entire base of the nacelle. (See section entitled "Corrections and Accuracies.")

The nacelles result in a slight forward movement of the aerodynamic center at the lowest test Mach number (2.29) and no change at a Mach number of 2.98. Plugging the upper nacelle causes a 3-percent forward

movement of the aerodynamic center at a Mach number of 2.29 and a barely detectable forward movement at a Mach number of 2.98.

Lateral Stability Characteristics

The lateral stability characteristics obtained in the present investigation are shown at approximately zero angle of attack in figure 11 and the variation of the lateral stability parameters with angle of attack in figure 12. The linearity of the results obtained at various angles of sideslip (fig. 11) indicate that the lateral stability parameters (fig. 12), obtained throughout the angle-of-attack range at nominal angles of sideslip of 0° and 5°, are a good representation of these characteristics at small angles of sideslip.

The results indicate that the primary effect of the nacelle-pylon installation is to substantially increase the directional stability of the wing due to the side area added by the nacelle installation aft of the balance moment center.

The effect of plugging one nacelle is to introduce an increment in yawing-moment coefficient that would require a change in trim of the configuration (fig. 11). The change in yawing moment is considered small in relation to the effect of the loss in thrust that such a condition would represent in the airplane.

In connection with the effect of plugging one nacelle, it will be recalled that the base pressure of the nacelle has been adjusted to a level of free-stream static pressure. Such a condition does not represent engine-out flight conditions wherein the base pressure could assume any value.

CONCLUDING REMARKS

The results of the investigation of the effect of nacelles on the aerodynamic characteristics of an 80° swept cambered and twisted wing indicate that the nacelles substantially reduce the maximum lift-drag ratio of the wing (from 7.3 to 4.0 at a Mach number of 2.98). This reduction in maximum lift-drag ratio is primarily the result of increased minimum drag. It is apparent that a change in inlet combination could reduce the drag penalty of the nacelles by reducing the wave drag and thus improve the lift-drag ratio of the wing-nacelle combination.

The nacelle-pylon combination increased the directional stability because of the rearward side area added to the wing. The primary effect

of plugging one nacelle, which represents a no-flow condition, is to introduce a small and probably trimmable increment in yawing moment.

Langley Research Center,
National Aeronautics and Space Administration,
Langley Field, Va., August 10, 1959.

REFERENCES

1. Hasson, Dennis P., Fichter, Ann B., and Wong, Norman: Aerodynamic Characteristics at Mach Numbers From 1.6 to 2.8 of 74° Swept Arrow Wings With and Without Camber and Twist. NASA TM X-8, 1959.

2. Hallissy, Joseph M., Jr., and Hasson, Dennis F.: Aerodynamic Characteristics at Mach Numbers of 2.36 and 2.87 of an Airplane Configuration Having a Cambered Arrow Wing With a 75° Swept Leading Edge. NACA RM L58E21, 1958.

3. Hasson, Dennis F., and Wong, Norman: Aerodynamic Characteristics at Mach Numbers From 2.29 to 4.65 of 80° Swept Arrow Wings With and Without Camber and Twist. NASA TM X-175, 1959.

4. Loving, Donald L., and Katzoff, S.: The Fluorescent-Oil Film Method and Other Techniques for Boundary-Layer Flow Visualization. NASA MEMO 3-17-59L, 1959.

TABLE I.- GEOMETRIC CHARACTERISTICS OF THE MODEL

Body:	
Length, in.	33.86
Maximum width, in.	1.37
Maximum height, in.	1.89
Base area, sq in.	2.39
Wing:	
Area, sq ft	1.99
Span, in.	17.63
Aspect ratio	1.08
Taper ratio	0
Sweepback of leading edge, deg	80.00
Sweepback of trailing edge, deg	63.4
Total length in streamwise direction wing apex to wing tip, in.	50.00
Mean aerodynamic chord, in.	21.67
Mean-aerodynamic-chord location, in. -	
Lateral location	2.94
Longitudinal location from apex	16.67
Notch ratio, $\frac{\text{Theoretical root chord}}{\text{Total length of wing}}$	0.65
Nacelle:	
Length, in.	9.90
Maximum diameter, in.	2.10
Exit diameter, in.	1.42
Inlet diameter, in.	1.40
Lip angle, deg	26.0
Base diameter, in.	1.75

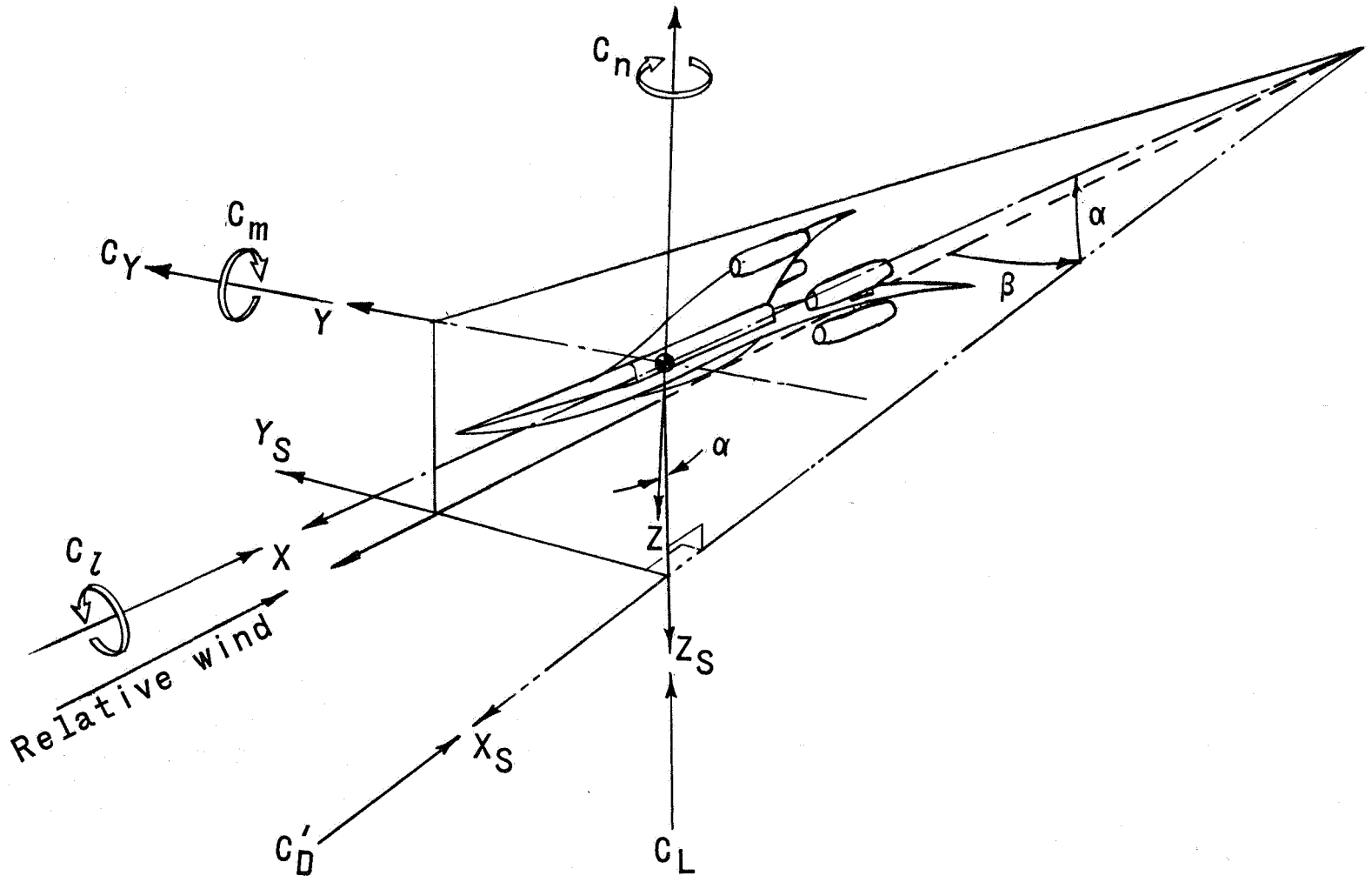

Figure 1 - [illegible]s system. Positive values of forces, moments, and angles are indicated by arrows.

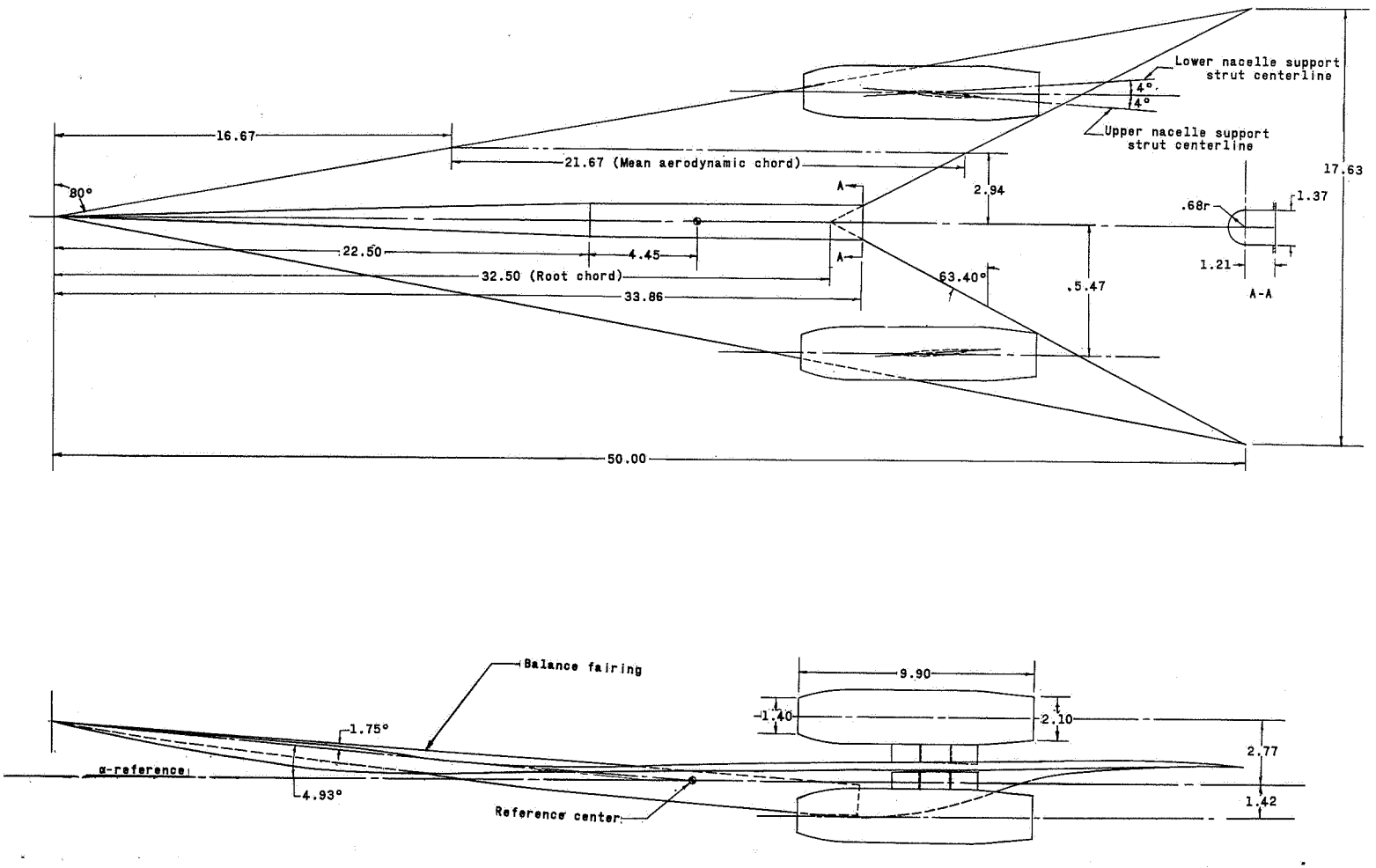

Figure 2.- Model drawing of twisted and cambered 80° swept arrow wing with nacelles. All dimensions are in inches unless otherwise noted.

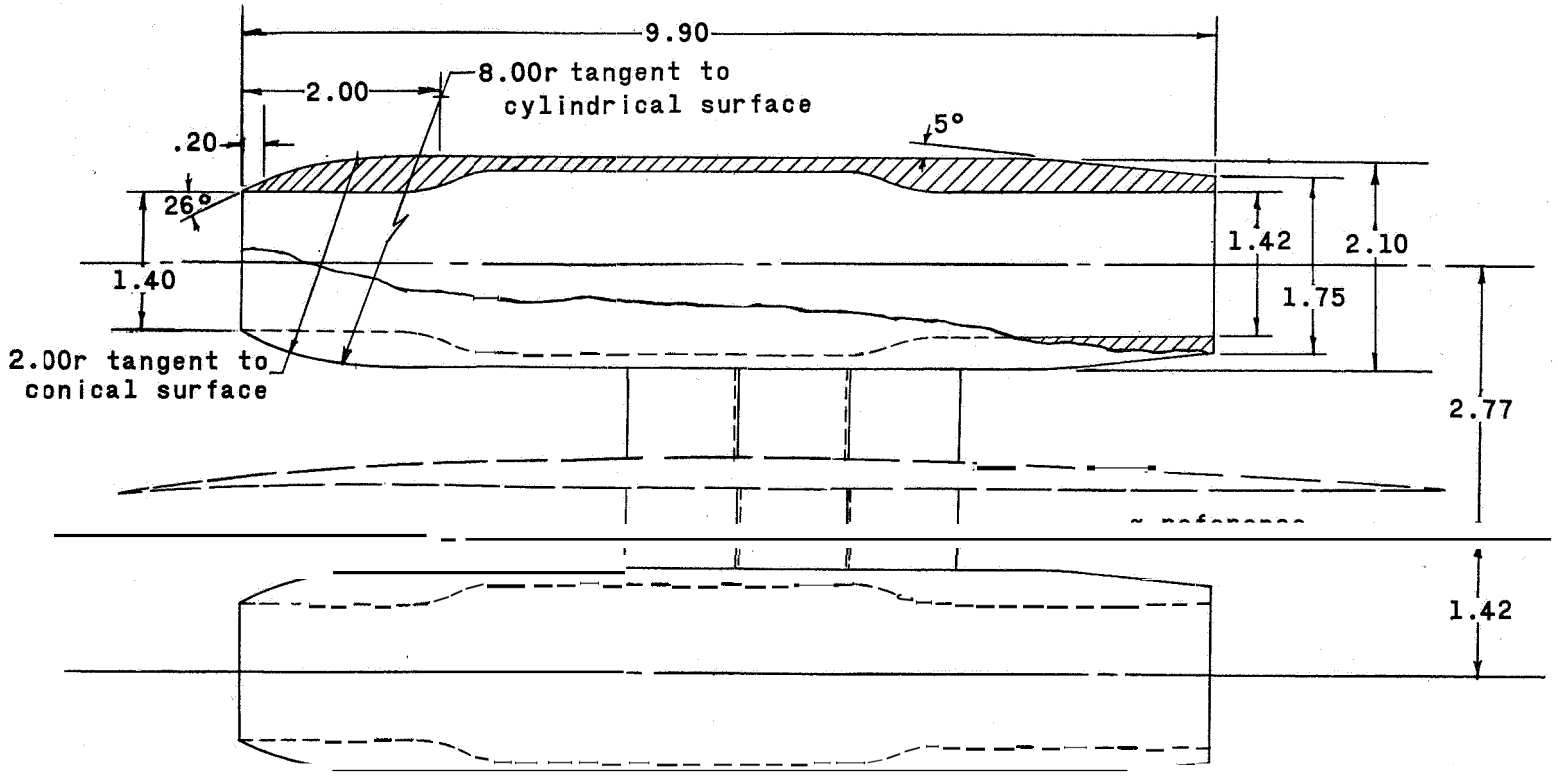

Figure 3 - Details of engine nacelles. All dimensions are in inches unless otherwise noted

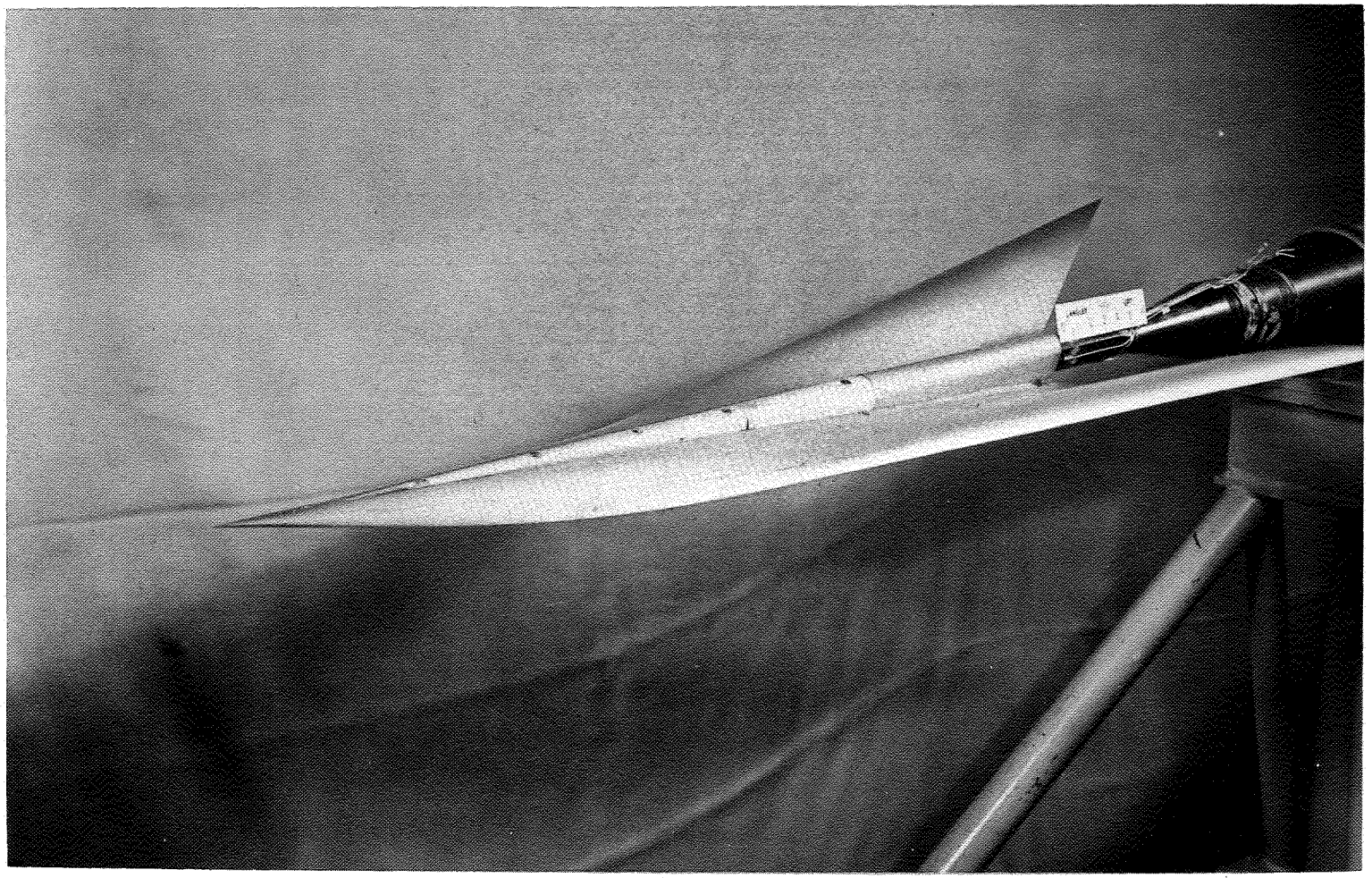

Figure 4.- Photograph of twisted and cambered 80° swept arrow wing. L-59-75

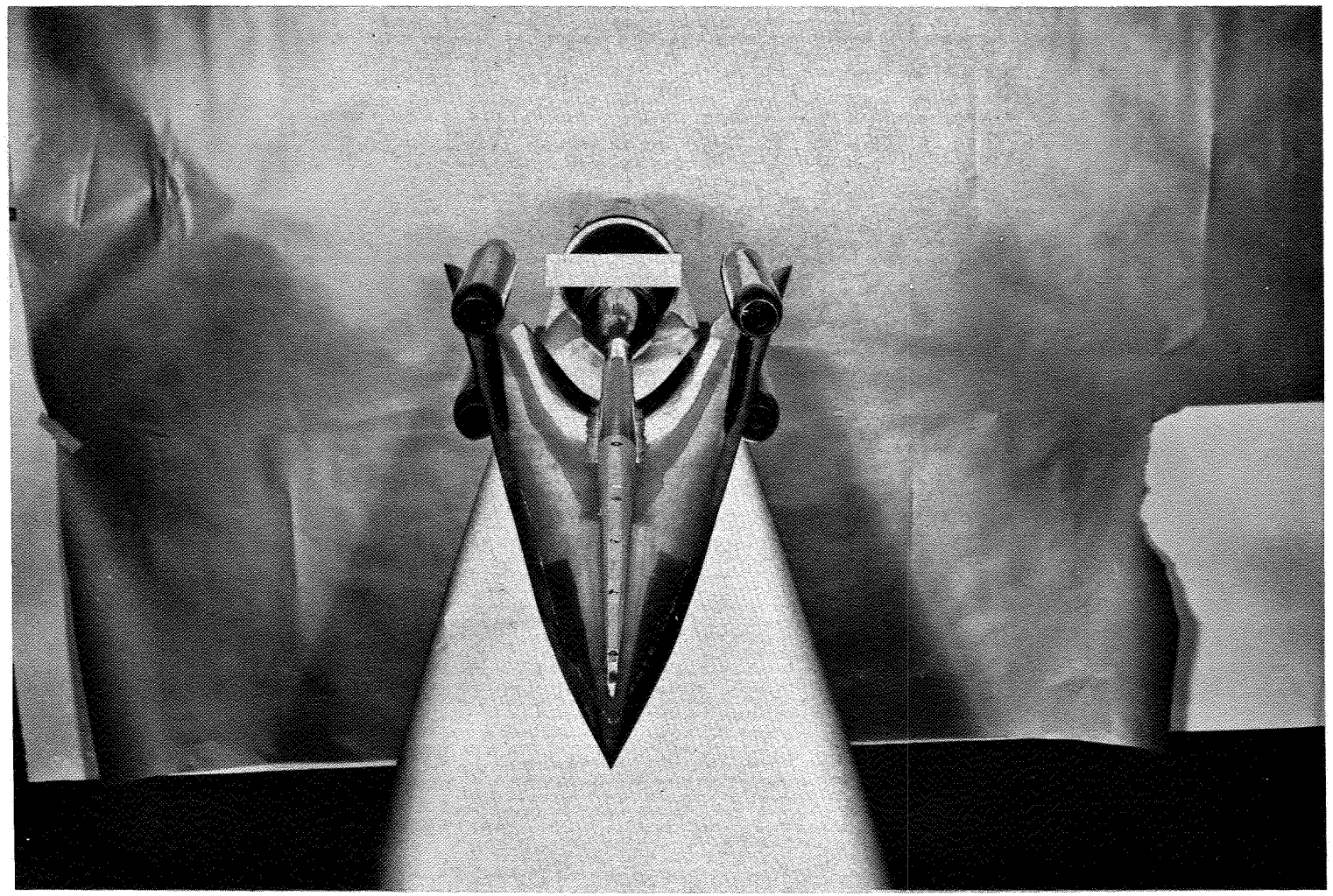

(a) Front view. L-59-3455

Figure 5 - Photographs of twisted and cambered 80° swept arrow wing with nacelles

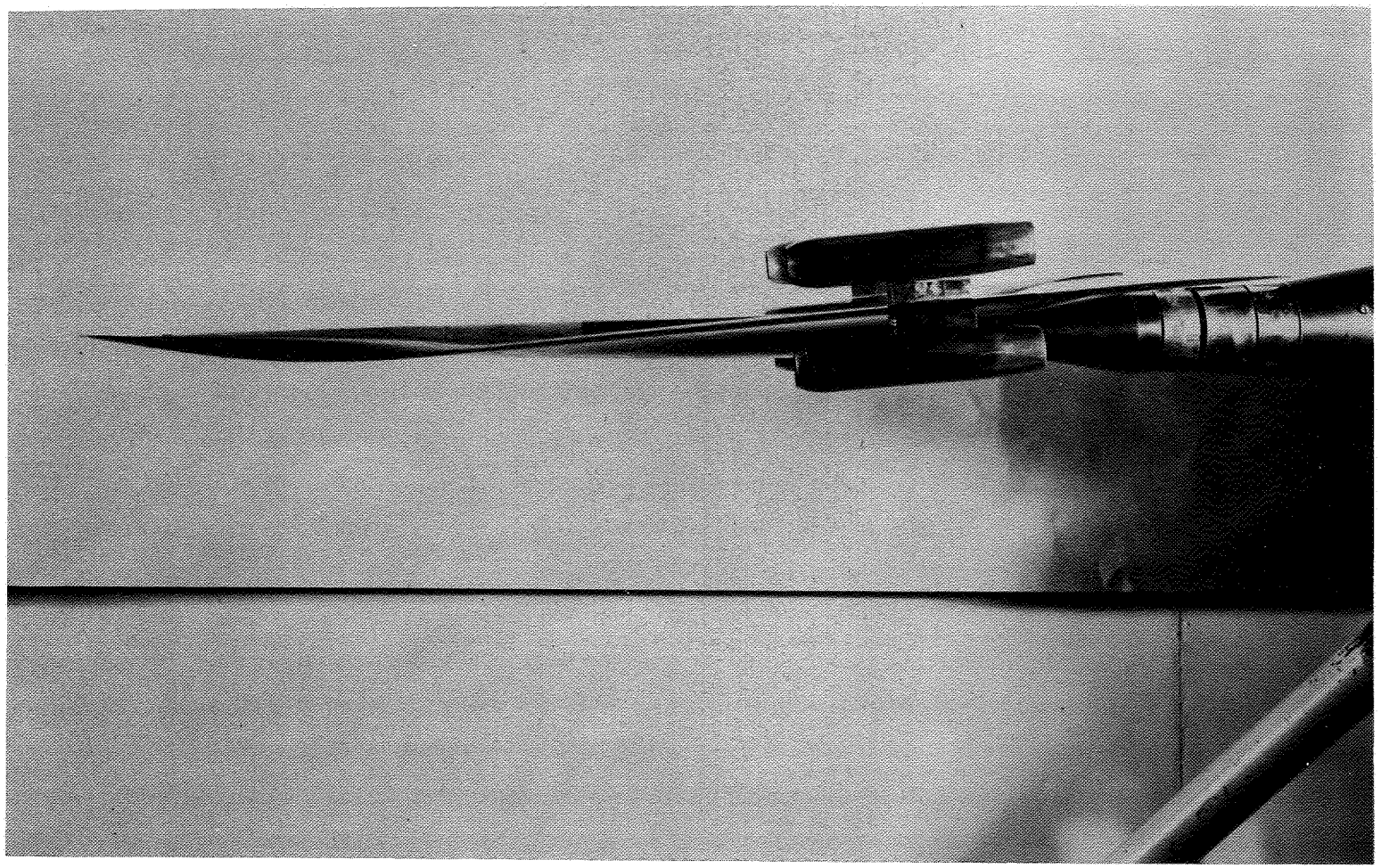

(b) Side view. L-59-3458

Figure 5 - Continued.

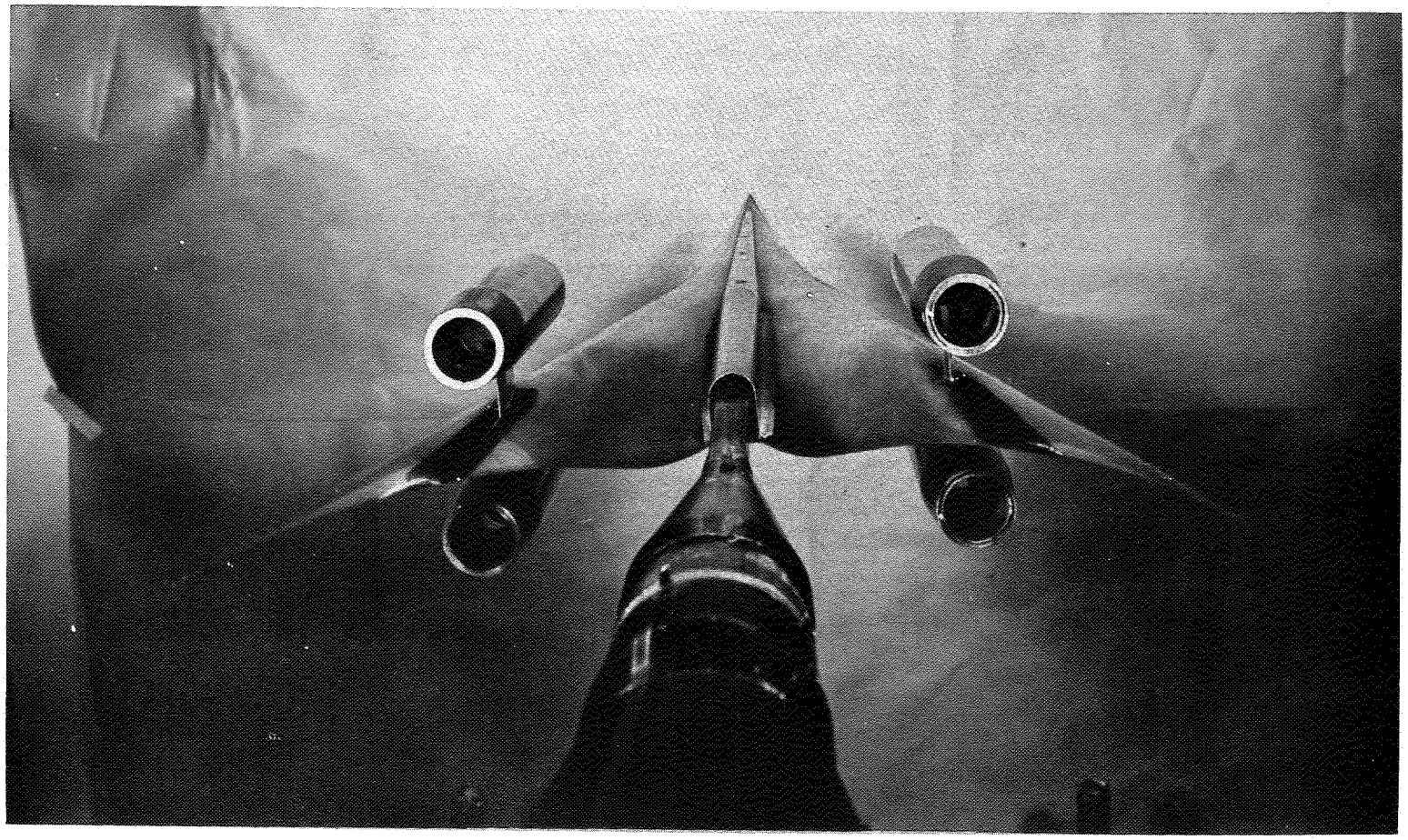

(c) Rear view. L-59-3457

Figure 5.- Concluded.

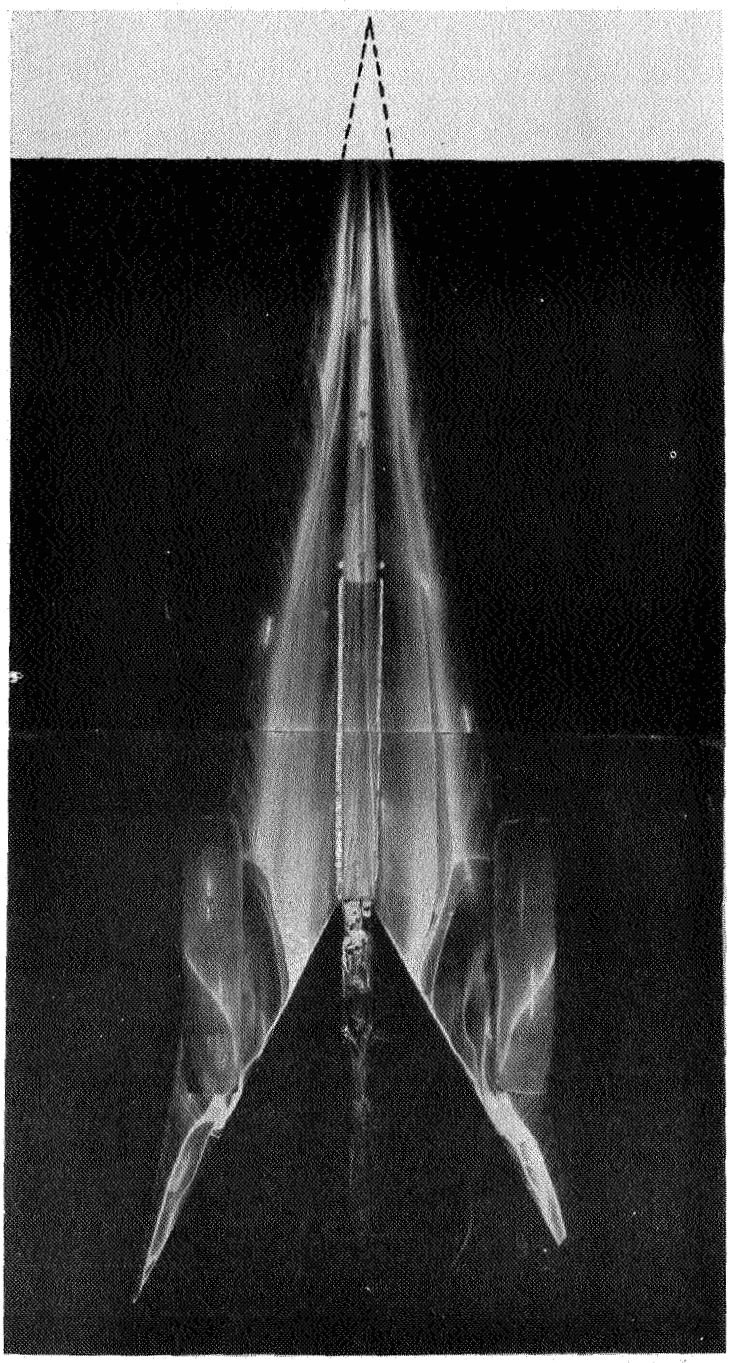

L-685

L-59-5051

Figure 6.- Oil-film flow photograph of the twisted and cambered 80° swept arrow wing with nacelles. Transition fixed; $R = 4.5 \times 10^6$; $C_L \approx -0.10$; $M = 2.98$.

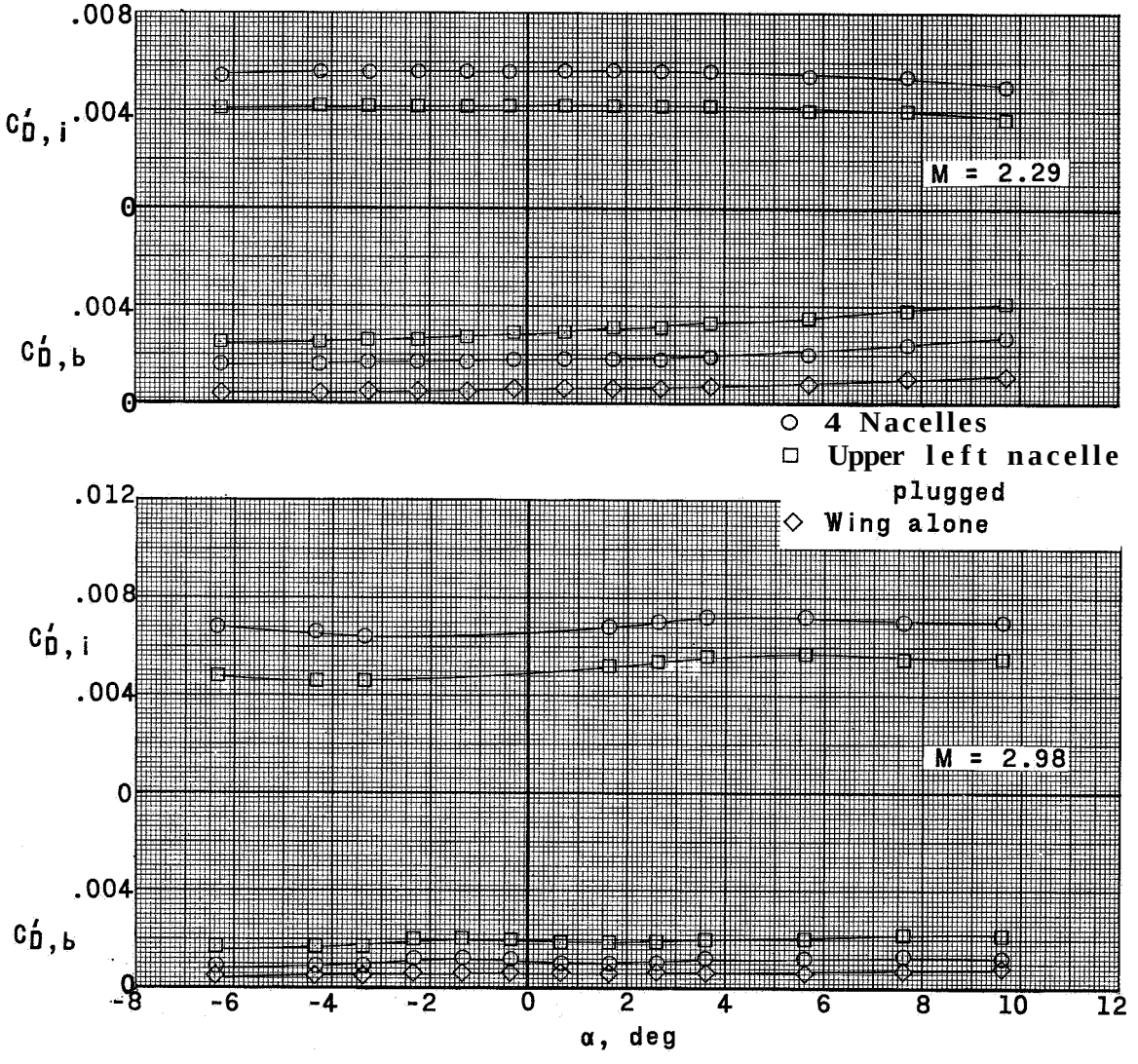

Figure 7.- Variation of base drag coefficient and internal drag coefficient for the twisted and cambered 80° swept arrow wing with and without nacelles.

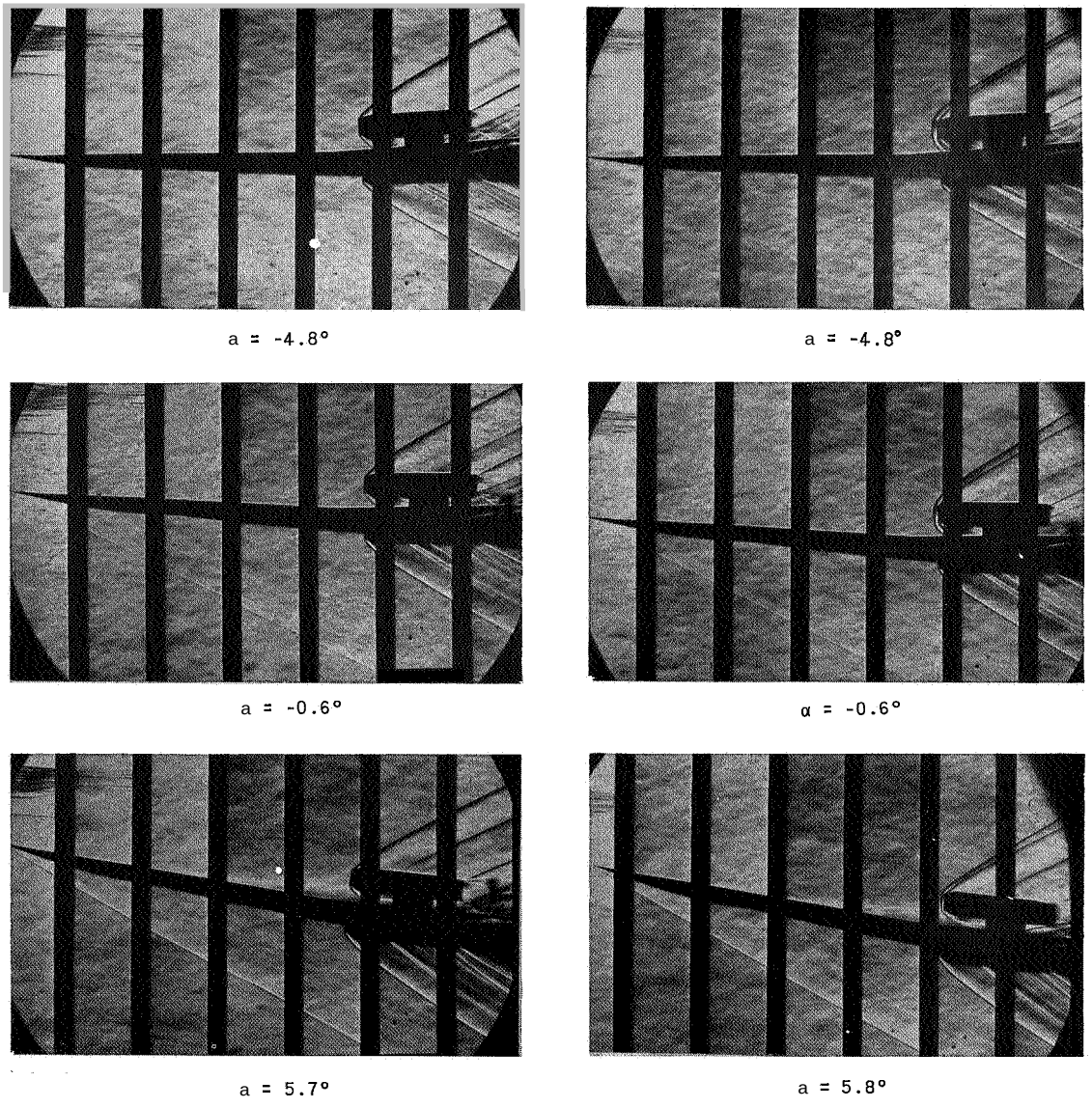

(a) M = 2.29.

L-59-5048

Figure 8.- Schlieren photographs of twisted and cambered 80° swept arrow wing with nacelles.

L-685

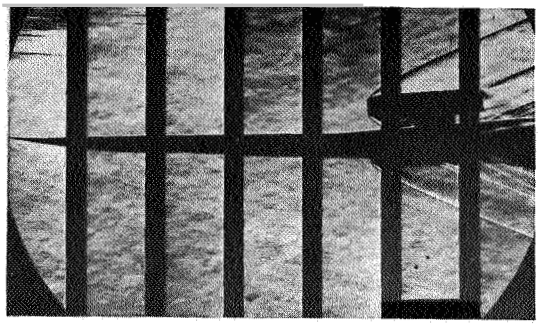

α = -5.0°

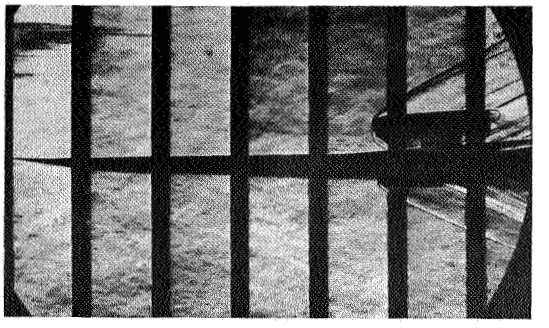

α= -4.4°

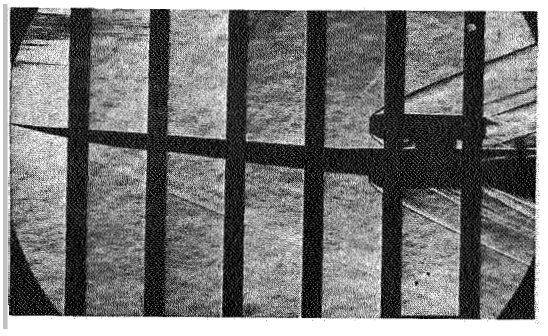

a = -0.8°

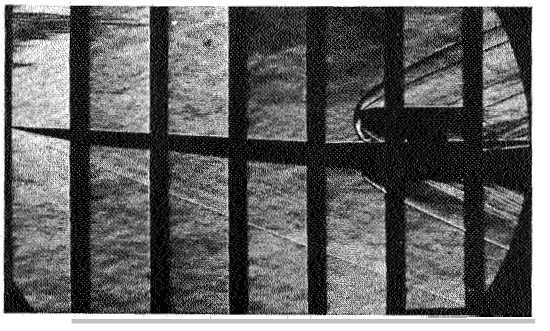

a = -0.40

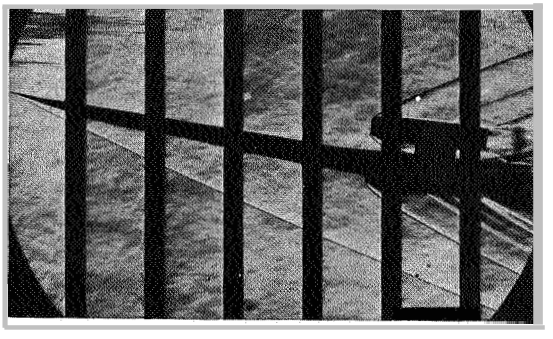

a = 5.5°

All nacelles open

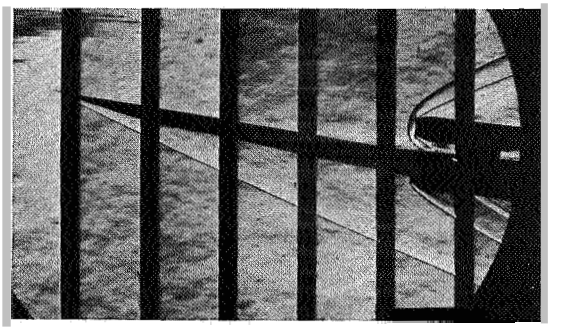

a = 5.6°

Upper left nacelle plugged

(b) M = *2.98.*

L-59-5049

Figure *8.-* Concluded.

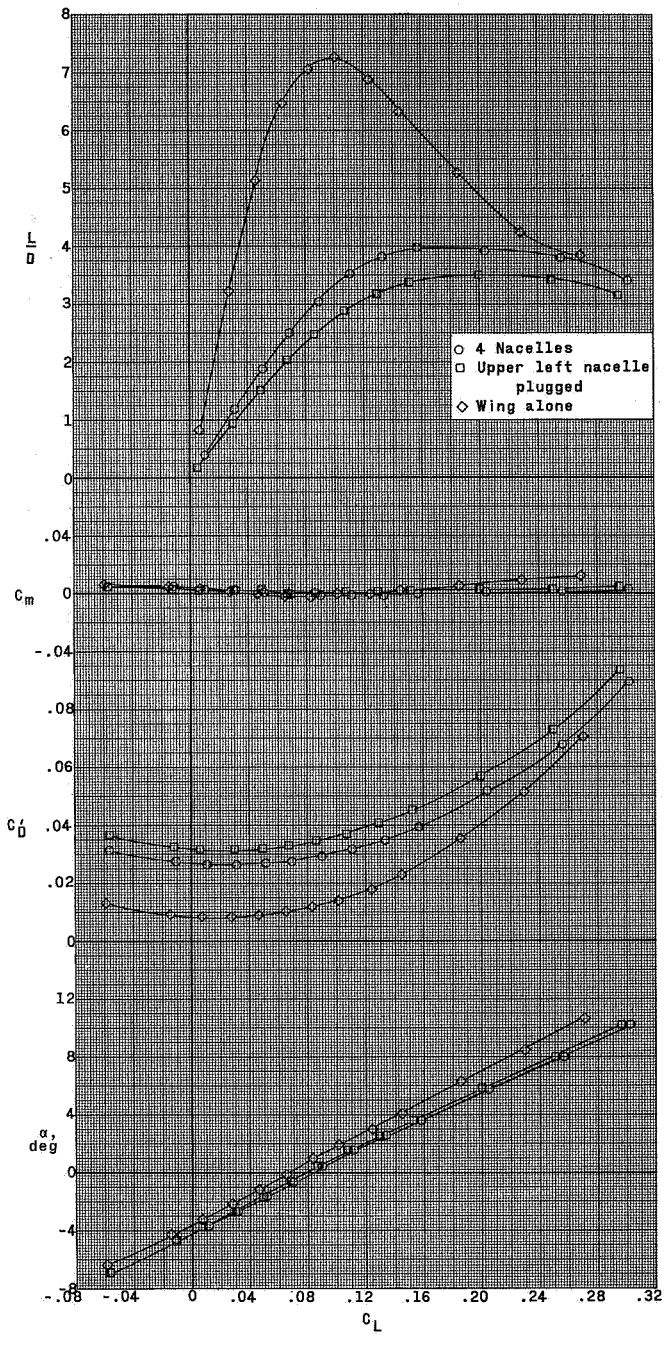

(a) M = 2.29.

Figure 9.- Effect of addition of nacelles and plugging of upper left nacelle on the longitudinal stability characteristics of a twisted and cambered 80° swept arrow wing. R = 4.5 x 10^6; β = 0°.

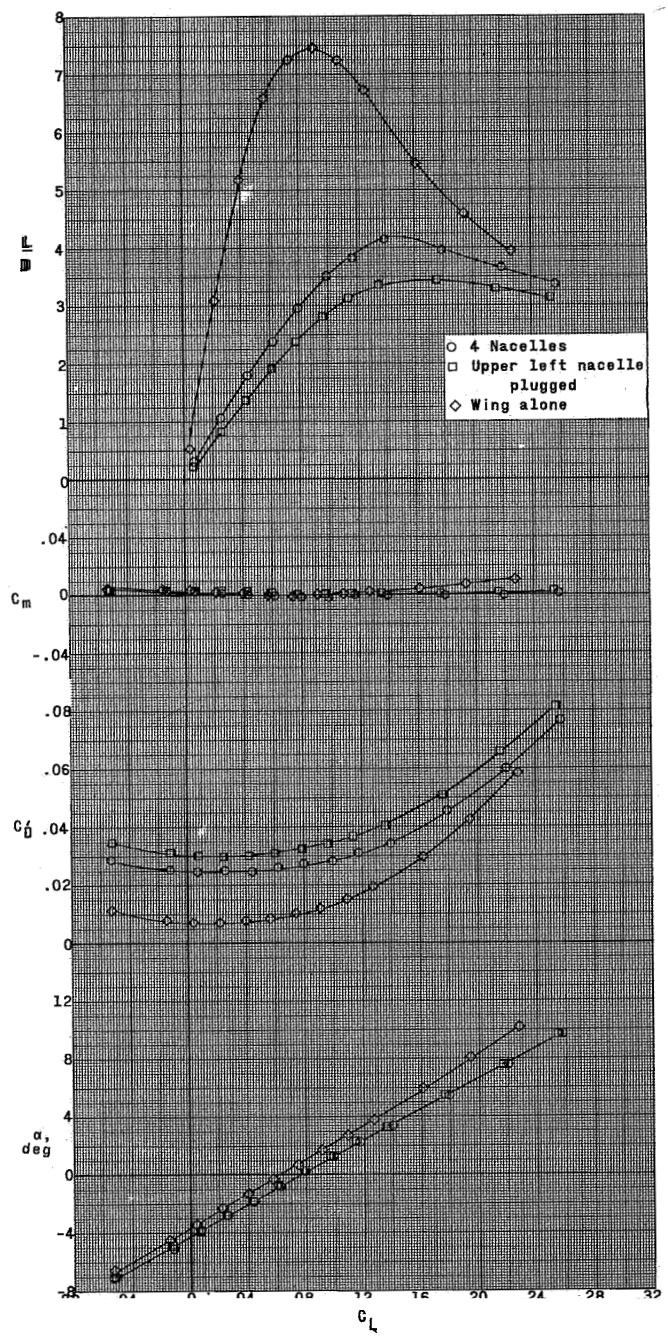

(b) M = *2.98.*

Figure 9.- **Concluded.**

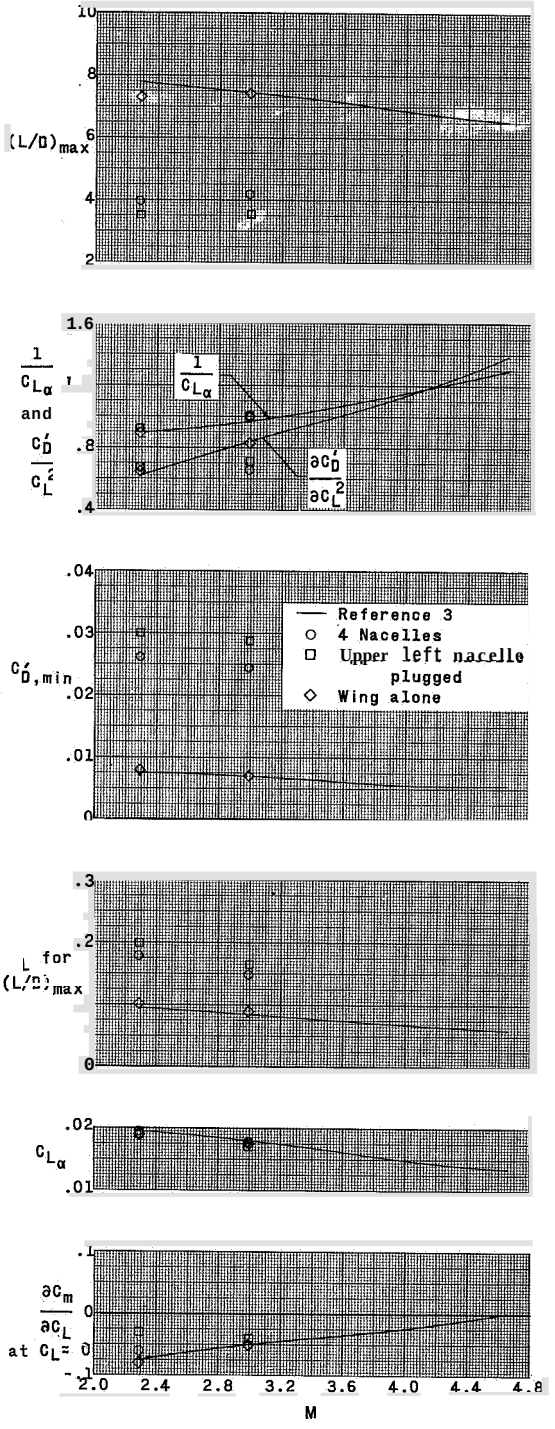

Figure 10.- Summary of the longitudinal stability characteristics of a twisted and cambered 80° swept arrow wing with nacelles.

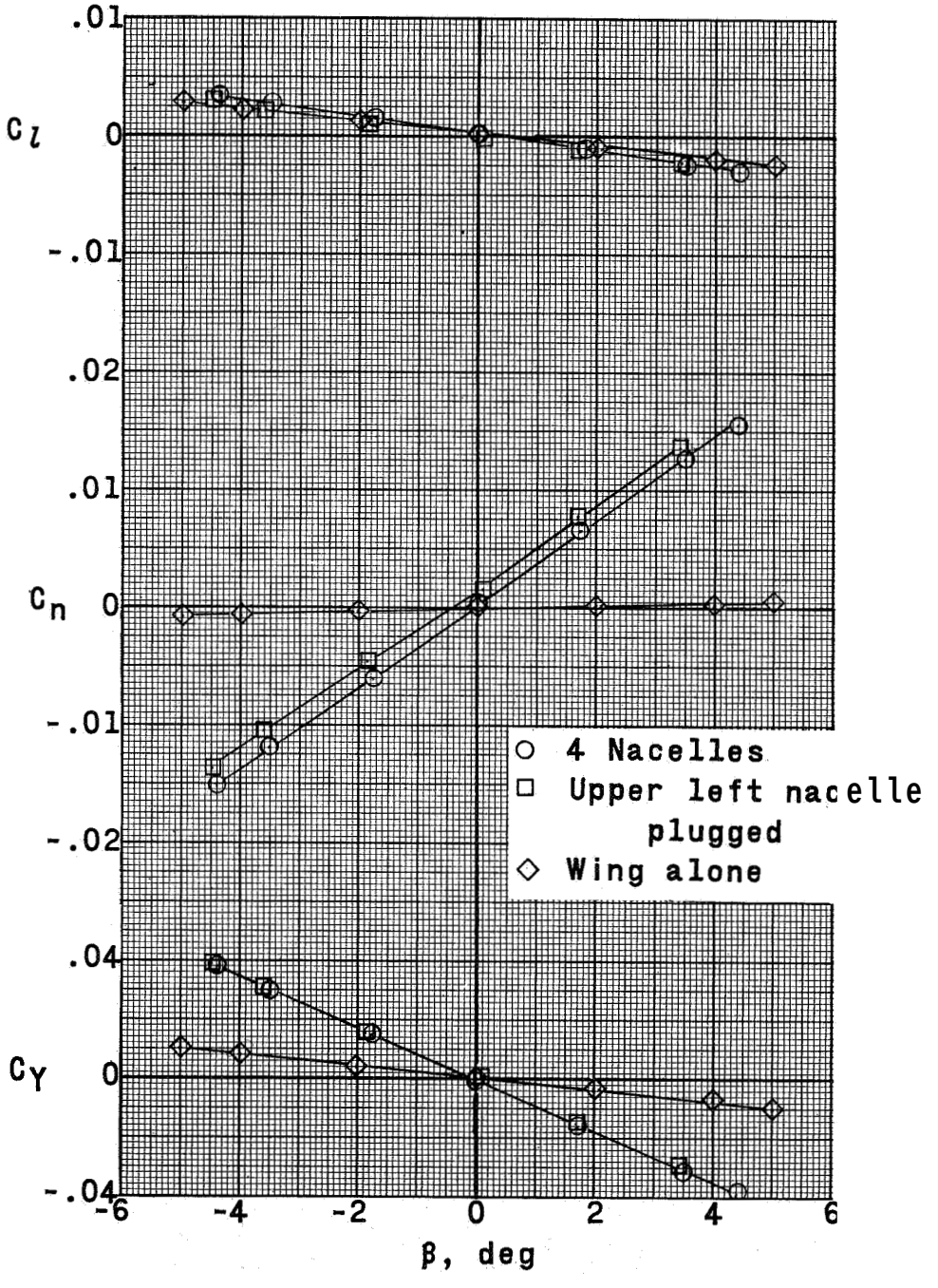

(a) M = 2.29.

Figure 11.- Effect of the addition of nacelles and plugging of the upper left nacelle on the lateral stability characteristics of a twisted and cambered 80° swept arrow wing. $R = 4.5 \times 10^6$; $\alpha \approx 0°$.

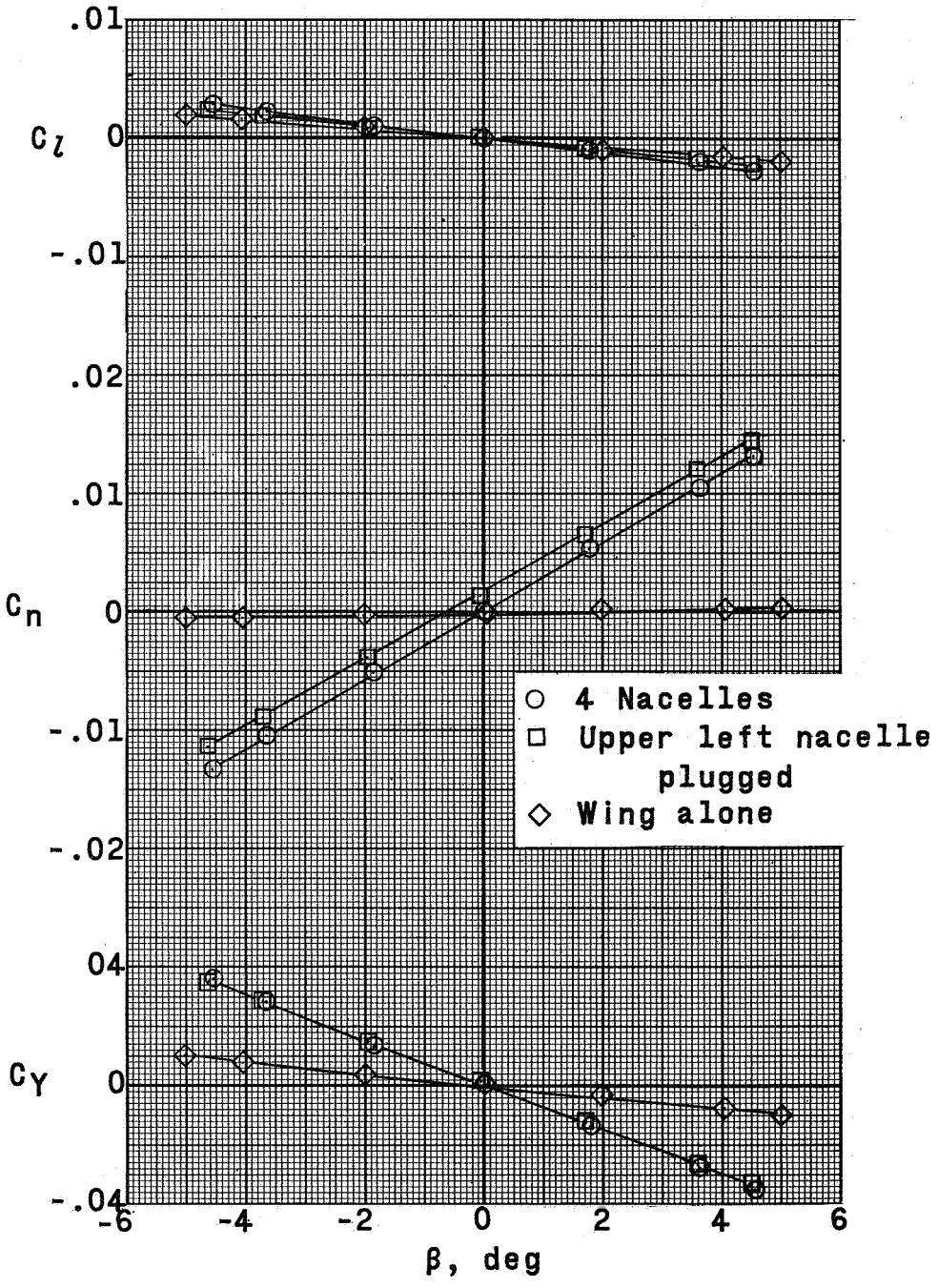

(b) M = 2.98.

Figure 11.- Concluded.

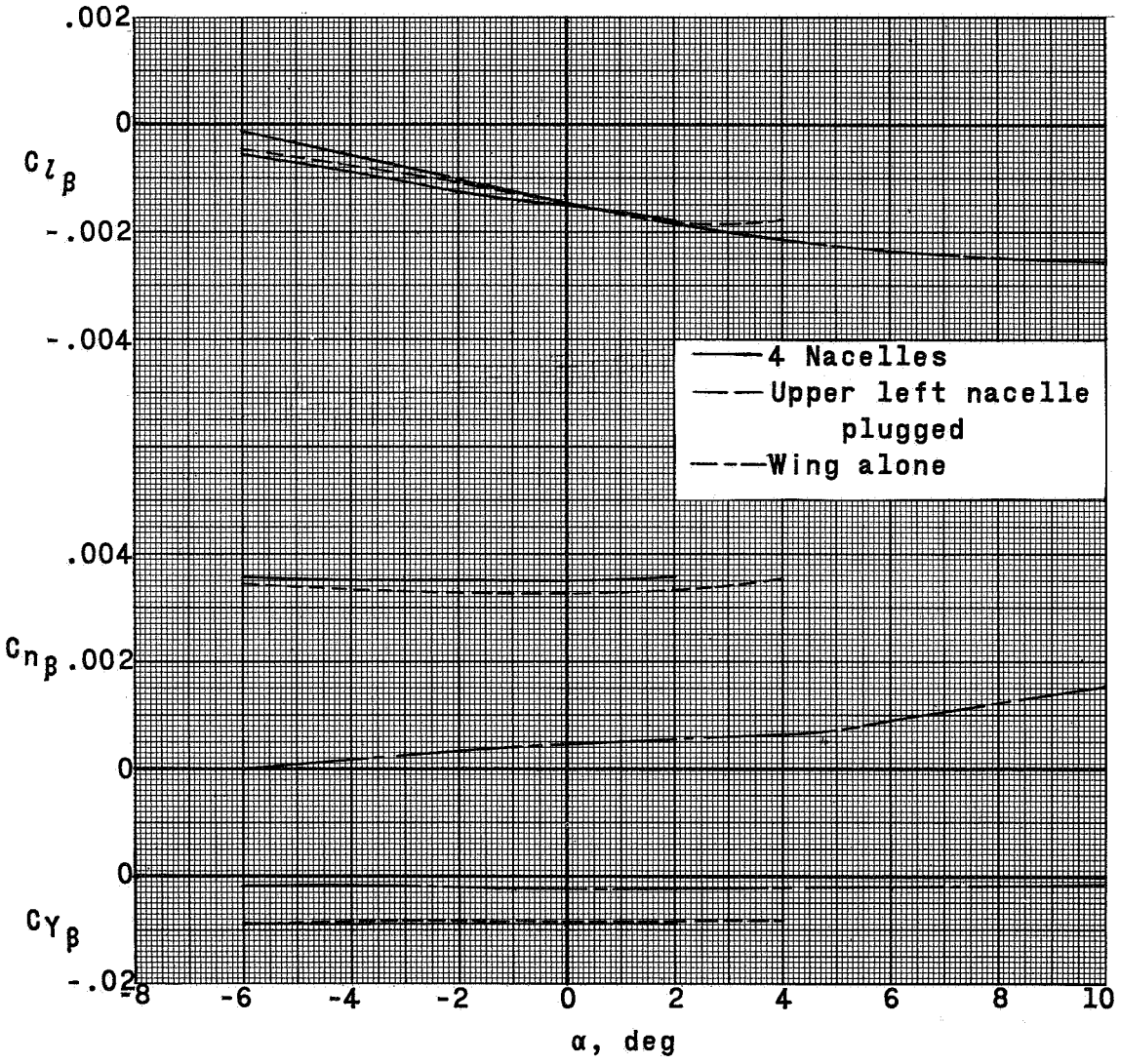

(a) M = 2.29.

Figure 12.- Summary of the lateral stability characteristics of a twisted and cambered 80° swept arrow wing with and without nacelles.

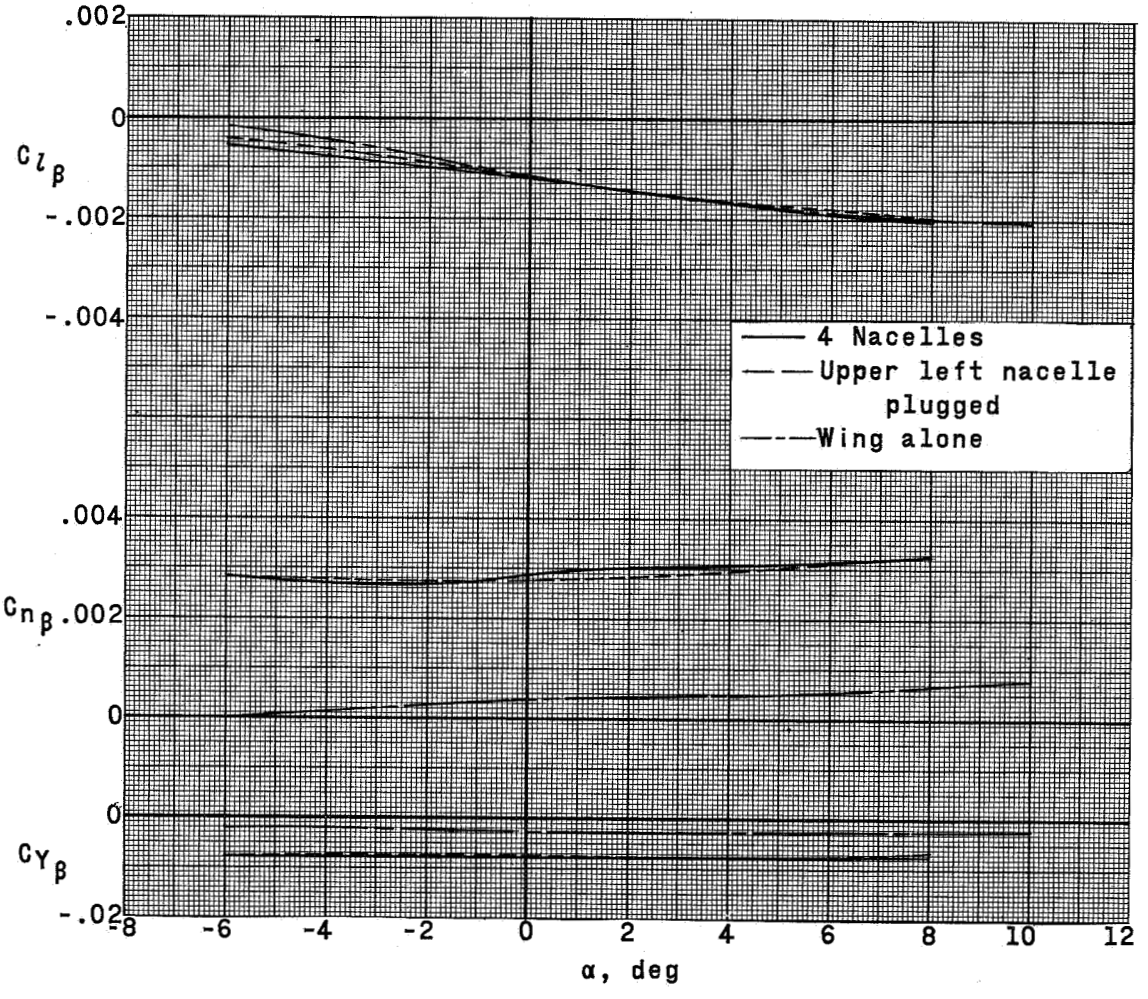

(b) M = 2.98.

Figure 12.- Concluded.

L-685